JOURNAL OF THERMOPHYSICS AND HEAT TRANSFER
Vol. 7, No. 1, Jan.–March 1993

Linear Pyrometer for Investigations of Thermal Protection Systems

O. R. Loesener,* M. Auweter-Kurtz,† M. Hartling,‡ and E. W. Messerschmid§
Institut für Raumfahrtsysteme, Universität Stuttgart, W-7000 Stuttgart 80, Germany

Simulated re-entry tests of reusable thermal protection systems for spacecraft are being conducted in an arc-heated, high-enthalpy wind tunnel. The operating conditions correspond to the early phase of re-entry. Steady-state operation of the test facility allows the determination of the material's performance. One of the most important measurement parameters for re-entry simulation is the material's front surface temperature, which has to be known as accurately as possible. The surface temperature is usually measured by remote pyrometers. Since the material is heated by the radiating plasma, signal disturbances are present when measuring through the plasma. Furthermore the normal spectral emittance is subject to changes, depending on the plasma conditions. In order to avoid these drawbacks which reduce accuracy, a new kind of pyrometer for the measurement of the rear side temperature was designed, where no disturbances by the plasma occur. It is integrated in the sample support system. The temperature range is 1200–2370 K and the measuring spot is 1 mm in diameter. This article describes the design and the application of the miniaturized pyrometer in the plasma wind tunnel.

Nomenclature

A = surface
C_{ge} = geometric factor
c_2 = second radiation constant
dA_i = infinitesimal surface-element for coordinate i
dF_{ij} = angle factor from dA_i to A_j
f = focal length
H = auxiliary function
I_{ph} = photocurrent (pyrometer signal)
$I_{ph,cal}$ = calibration photocurrent
L_λ = spectral radiance
$L_{\lambda,bb}$ = blackbody spectral radiance
M_λ = spectral radiant exitance
$M_{\lambda,bb}$ = blackbody spectral radiant exitance
n_i = number of cavity zones along wall i
s = responsivity
T = temperature
T_b = back surface temperature
T_{cal} = calibration temperature
T_f = front surface temperature
T_{Ki} = thermocouple temperatures
T_0 = reference temperature
ε = normal spectral emittance
ε_a = effective (apparent) spectral emittance
$\bar{\lambda}_{eff}$ = mean effective wavelength
τ_f = filter transmittance
τ_{gl} = glass window transmittance

Introduction

A RELIABLE simulation of the re-entry of a spacecraft into the Earth's atmosphere for analysis of the material erosion requires the duplication of the thermal load acting on the spacecraft.[1]

An arc-heated high-enthalpy wind tunnel is being used at the University of Stuttgart, Institut für Raumfahrtsysteme (IRS), as a test facility for the experimental investigation of the erosion behavior of materials for thermal protection systems of future spacecraft.[2,3] The re-entry corridor shown in Fig. 1 exhibits only a small range of possible trajectories during the first phase of re-entry, when the aerodynamic heating and the resultant surface temperatures are high. The erosion behavior of the materials at such high temperatures (up to about 1900 K) is very temperature dependent. Therefore during the simulation in a plasma wind tunnel, it is necessary to

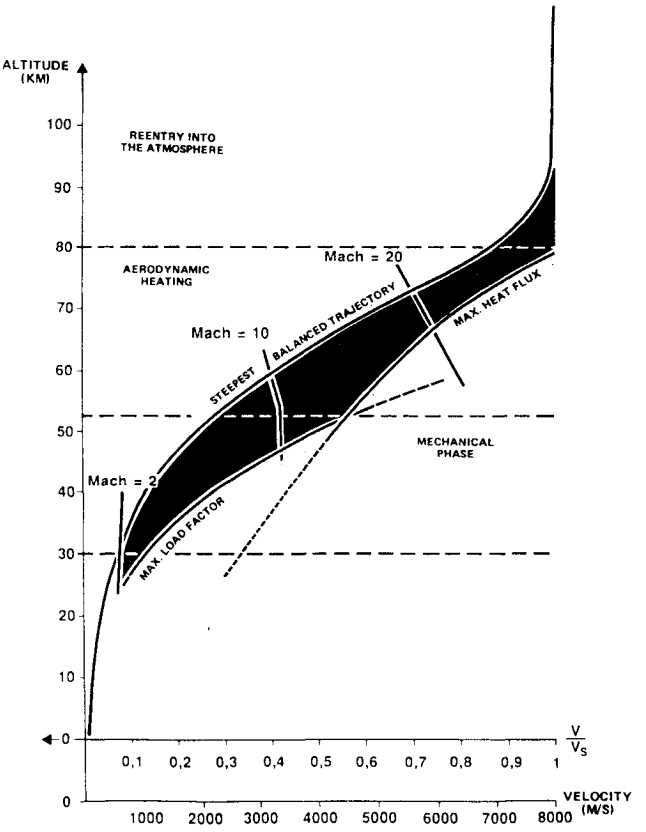

Fig. 1 Glider-like re-entry corridor.

Presented as Paper 91-1387 at the AIAA 26th Thermophysics Conference, Honolulu, HI, June 24–26, 1991; received Aug. 22, 1991; revision received Dec. 16, 1991; accepted for publication Dec. 17, 1991.

*Research Scientist, Electric Propulsion and Plasma Technology Division, Postfach 80 11 40. Senior Member AIAA.
†Professor, Head Electric Propulsion and Plasma Technology Division. Member AIAA.
‡Technical Staff Member, Electronics Division.
§Institute Director.

measure the true temperature of the thermal protection materials as accurately as possible.

For ablative materials the temperature measurement is performed with thermocouples.[5] However, this method cannot be used for radiation-cooled materials such as fiber-reinforced ceramics, because of chemical reactions (carbidization) and insufficient thickness (only 1–2 mm). Modern radiation-cooled materials based on silicon carbide (SiC) and/or carbon (C) have low mass and high emittance at high temperatures (about 0.80 or higher) and show good resistance to withstand reentry conditions.[6,7] Pyrometers have the advantage of being nonintrusive and contactless optoelectronic devices, which are therefore best suited to perform such measurements. These pyrometers are standard devices, which operate with silicon photodiodes in the visible and near infrared spectral range. Nevertheless the heating plasma radiates in the spectral range where the temperature is measured and disturbs the temperature measurement made through it. Such disturbances can be taken into account when a linear pyrometer is used;[8] however, the correction terms provided by emission and absorption spectroscopy depend on the operating conditions, like specific enthalpy, ambient pressure in the plasma wind tunnel, plasma density, and plasma composition. The investigation of these correction terms is very time consuming due to the large number of variables involved. Furthermore the normal spectral emittance of such new materials is not well known and is subject to changes with time under a high-enthalpy plasma load. A material surface change due to chemical effects causes a change in the emittance, so that an apparent surface temperature change is observed when making long-term experiments. In order to avoid these problems which inevitably reduce the accuracy, a new kind of pyrometer for surface temperature measurement was designed, which is integrated in the water-cooled sample support system. Since the rear side of the material is not disturbed by the plasma load, no emittance changes occur at all. An effective emittance must be calculated in order to consider the radiation exchange between the sample and its surroundings (support system). This effective emittance will always be higher than the normal spectral emittance of the material. Results achieved in the plasma wind tunnel are discussed below.

Design

There are some general rules to be considered as design criteria.[9]

The design parameters were selected as follows:

1) The device has to be as small as possible so that it can be placed inside the well-cooled sample support system designed for material experiments for the HERMES program. These experiments are stagnation point experiments with samples 25 mm in diameter which have a thickness of a few millimeters.[10] To make sure that the measurement is not influenced by the plasma, care must be taken to guarantee good mechanical stability.

2) The temperature range for the minipyrometer of 1275–2175 K was chosen mainly in accordance with the simulation requirements for spacecraft like HERMES.[11]

3) A measuring rate of 10 s^{-1} with an accuracy of 0.2% was aimed at matching the values obtained on the first Space Shuttle missions, where the temperature history during reentry was measured by means of thermocouples, and the maximum gradient was shown to be 6.5 K/s.[12] Similar values are expected for HERMES.[13]

The pyrometer and its water-cooled housing are shown schematically in Fig. 2. First the water cools the front part of the housing where the optical components are placed; it is then guided to the electronic part at the rear of the support system. The water-cooled housing has metallic components only; its inner part is coated with a special flat black paint (Pyromark 2500) to avoid stray light in the light track.[14]

An easy-to-replace glass window (W) is placed at the optics entrance to avoid immediate instrument destruction, if the sample fails. A biconvex lens (L) (f = 43 mm) forms the imaging optics, which show minimal aberration effects with a magnification of unity. To avoid reflections between optical components, the lens with a broadband antireflexion coating was chosen. Besides the aperture stop (A, 8 mm) other baffles (S) were inserted into the light path to further suppress scattering light sources. The measuring spot is 1.1 mm in diameter, given by the selected detector.

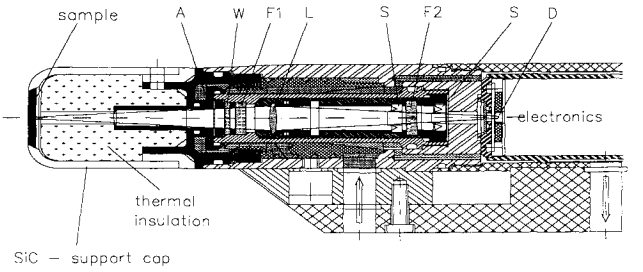

Fig. 2 Schematic view of the pyrometer head.

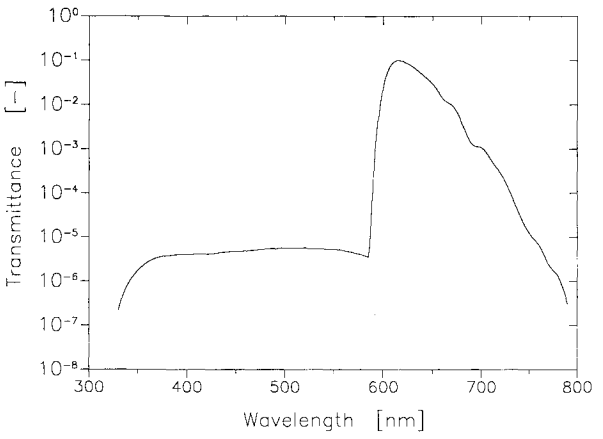

Fig. 3 Spectral transmittance of the filter.

To achieve the desired accuracy it is necessary to operate the device at short wavelengths (380–780 nm). The slope of spectral radiance is highest at short wavelengths, therefore the shorter the wavelength the better the device sensitivity.[15]

A combination of colored glasses (F1 = KG5; F2 = BG18, RG610) was chosen to achieve a good mechanical as well as thermal stability within the desired wavelength range. Furthermore this combination yields a very small residual transmission for longer wavelengths between 800 and 1140 nm, which allows a small margin of error.[16] An imperfect blocking behavior of a filter can cause large errors in pyrometry.[17,18] This has been taken into account when designing the device. The resulting spectral transmittance curve is shown in Fig. 3.

The performance of a pyrometer is mainly determined by the choice of both the filter and the detector. Therefore a detector should be selected on the basis of its sensitivity, linearity, noise, temperature, and time stability. Linearity means that the radiance of the source is proportional to the output signal of the detector. Silicon photodiodes are well-suited for use as detectors in pyrometric applications, because of their high sensitivity and stability.[19] Figure 4 depicts the spectral responsivity of the chosen photodiode. This photodiode shows high sensitivity, high-series resistance, good linearity, and temperature coefficient. To avoid thermal drifts in the signal, the photodiode is temperature-stabilized by Peltier devices. The photodiode (D) acts as a field stop.

Using the optical components and detector specifications taken from data sheets, the calculation of the photocurrent I_{ph} is possible by solving the following integral[20]:

$$I_{ph} = C_{ge} \int L_{\lambda,bb}(\lambda, T) s(\lambda) \tau_f(\lambda) \tau_{gl}(\lambda)\, d\lambda \qquad (1)$$

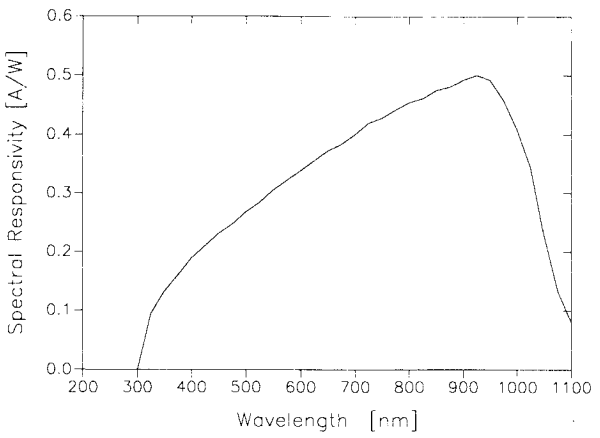

Fig. 4 Spectral responsivity.

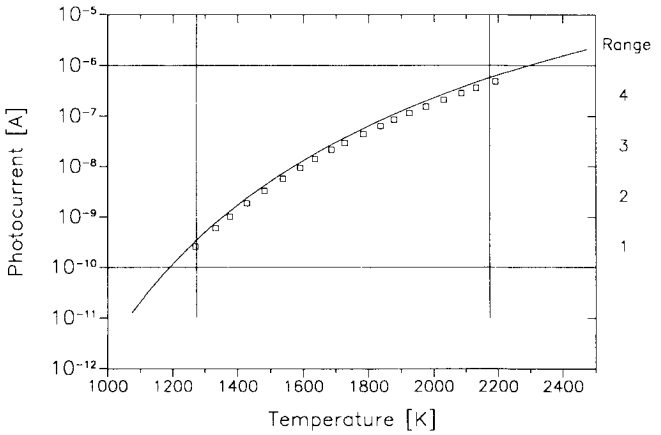

Fig. 5 Calculated (——) and measured (□) photocurrent I_{ph} as a function of the temperature T.

which yields the photocurrent as a function of the temperature range for a blackbody (see Fig. 5).

Figure 5 shows that the usable photodiode measuring range lies between 0.1 nA and 1 μA. This curve is valid only if both the switching network with high impedance character and the amplifier show good noise properties and high stability. In this device these conditions are fulfilled.

The photocurrent is measured in a standard transimpedance circuit using an operational amplifier and four feedback resistors which can be switched manually. The selection of these components was supported by calculations of the equivalent input noise current, which were further useful in determining the contribution to the measuring error from the electronics expressed in a signal-to-noise ratio.

Calibration

The miniaturized pyrometer was calibrated with a blackbody source[21] and an accurate photoelectric pyrometer,[22] between 1270–2200 K, to verify both the linearity and the accuracy over the whole measuring range.

The blackbody source itself works between 1075–3000 K, with an effective emittance of $\varepsilon(\lambda, T) = 0.995 \pm 0.005$. The ripple of temperature is less than ±0.5 K. A graphite rod with a cylindrical hole (ø15 mm, 128 mm) forms the cavity. The rod is electrically heated and can be operated in vacuum and in an argon atmosphere, depending on the temperature to be achieved. A glass window with a transmittance of $\tau_{gl} = 0.927$ is needed to operate the blackbody source.

The photoelectric pyrometer was used to measure the temperature of the blackbody source at a wavelength of (651.05 ± 0.20 nm).

For geometrical reasons an auxiliary lens was used to allow correct imaging of the cavity wall, which corresponds to the surface of the heated sample on the pyrometer entrance.

The calibration curve of the miniaturized pyrometer is depicted in Fig. 5.

The agreement of both curves is quite satisfactory, deviations occur due to inaccuracies in the manufacturing of the components.

The temperature measuring range extends from almost 1200 to over 2370 K.

Temperature Calculation

The temperature in precision pyrometry is calculated from the ratio between measurement and calibration signal[23]:

$$Q = \frac{I_{ph}(T)}{I_{ph,cal}(T_{cal})} = \frac{\int \varepsilon(\lambda, T) L_{\lambda,bb}(\lambda, T) s(\lambda) \tau_f(\lambda) \tau_{gl}(\lambda)\, d\lambda}{\int L_{\lambda,bb}(\lambda, T_{cal}) s(\lambda) \tau_f(\lambda) \tau_{gl}(\lambda)\, d\lambda} \tag{2}$$

This equation must be solved with respect to T for temperature determination, either directly by using an iterative procedure (which is very time consuming) or by using approximate expressions, like the one suggested by Jung and Verch[24]

$$H(T) = a + (b/T - c) \tag{3}$$

where $a = -3.80$, $b = -23{,}108.66$ K, and $c = -13.0$ K.

This function is an expression for the logarithm of the integral representing the signal; its coefficients were calculated for the miniaturized pyrometer. This yields the following equation for temperature determination:

$$T = c + \left[\frac{1}{b} \ln \frac{I_{ph}}{\varepsilon I_{ph,cal}} + \frac{1}{T_{cal} - c}\right]^{-1} \tag{4}$$

which is more suitable for this application.

The accuracy of the expression for the temperature evaluation, device linearity, and blackbody source-stability is shown in Fig. 6.

The mean effective wavelength of the miniaturized pyrometer can be described in terms of the coefficients b and c (see Fig. 7):

$$\bar{\lambda}_{eff}(T, T_{cal}) = -\frac{c_2}{b} \frac{(T - c)(T_{cal} - c)}{T T_{cal}} \tag{5}$$

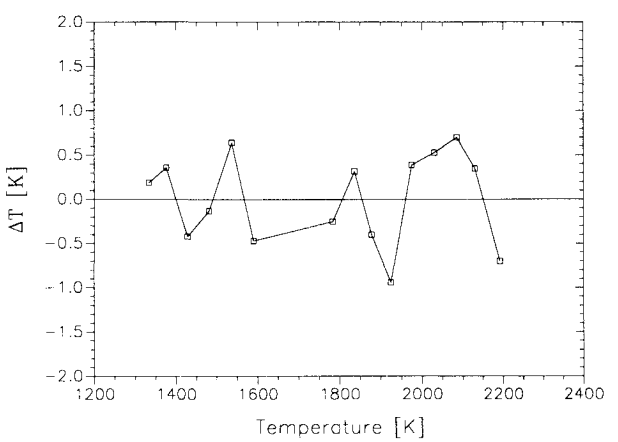

Fig. 6 Differences between calibration temperature of the calibration pyrometer and evaluated temperature for the miniaturized pyrometer as a function of the calibration temperature.

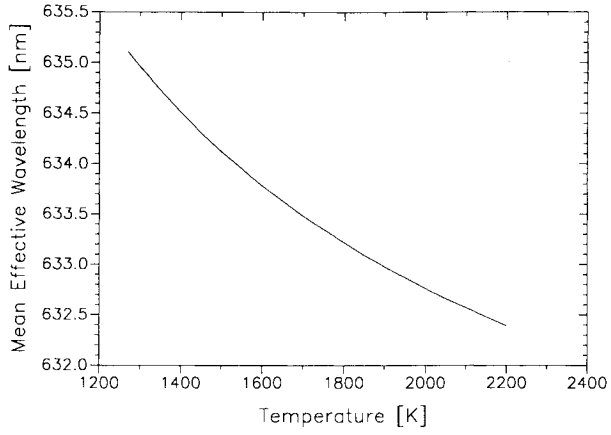

Fig. 7 Effective wavelength as a function of the temperature (referred to the gold freezing point).

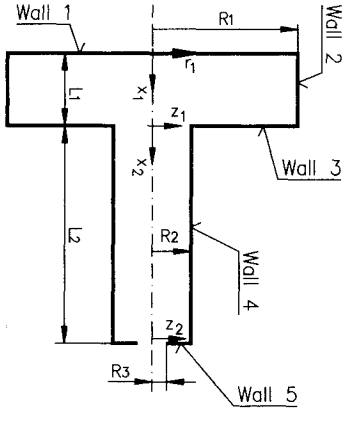

Fig. 8 Schematic view of the cavity. Wall 1 = rear side of the sample; Wall 2 = support cap; Walls 3 and 4 = insulation ceramics; Wall 5 = copper diaphragm; and $L1$ = 1.6 mm, $L2$ = 27 mm, $R1$ = 13 mm, $R2$ = 6 mm, $R3$ = 2.4 mm. The notation was chosen according to Ref. 25.

Emittance

For precise radiation pyrometry the material's emittance is needed, which describes the ratio of the radiant exitance of the specimen to that emitted by a blackbody radiation at the same temperature and under the same geometry and wavelength conditions. As the pyrometer works at 633 nm and the measurement is performed perpendicular to the specimen, the normal spectral emittance must be used. Furthermore due to the cavity configuration, the thermal radiation characteristics of the sample change (see Figs. 2 and 8).

The radiation characteristics of the enclosure can be determined by taking into account the radiative interchanges inside it. This means that one has the problem of finding the effective spectral emittance distribution in a nonisothermal diffuse cylindrical cavity.[25]

The nonisothermal effective spectral emittance ε_a of dA_{x2} is defined as the ratio of the spectral radiant exitance of dA_{x2} at temperature T_{x2} and the spectral radiant exitance of a blackbody at temperature T_0, as given by the Planck law

$$\varepsilon_a(x2, \lambda, T_{x2}, T_0) = \frac{M_\lambda(x2, \lambda, T_{x2})}{M_{\lambda,bb}(\lambda, T_0)} \tag{6}$$

The spectral radiant exitance of dA_{x2} has two components, corresponding to the emitted radiation and the reflected incident radiation.[26] The latter component yields in this case four terms. The overall radiative interchanges will be described by a set of five integral equations.

The equation of the effective spectral emittance of the sample (rear side) then becomes

$$\varepsilon_a(r1) = \varepsilon_{w1} \cdot \left[\frac{\exp(c_2/\lambda T_0) - 1}{\exp(c_2/\lambda T_{r1}) - 1}\right] + (1 - \varepsilon_{w1}) \cdot \left\{ \sum_{j=1}^{n2} \frac{1}{2} [\varepsilon_a(x1_{j+1}) + \varepsilon_a(x1_j)] \cdot (dF_{r1,x1_j} - dF_{r1,x1_{j+1}}) + \sum_{k=1}^{n3} \frac{1}{2} [\varepsilon_a(z1_{k+1}) + \varepsilon_a(z1_k)] \cdot (dF_{r1,z1_{k+1}} - dF_{r1,z1_k}) + \sum_{l=1}^{n4} \frac{1}{2} [\varepsilon_a(x2_{l+1}) + \varepsilon_a(x2_l)] \cdot (dF_{r1,x2_l} - dF_{r1,x2_{l+1}}) + \sum_{m=1}^{n5} \frac{1}{2} [\varepsilon_a(z2_{m+1}) + \varepsilon_a(z2_m)] \cdot (dF_{r1,z2_{m+1}} - dF_{r1,z2_m}) \right\} \tag{7}$$

where the wavelength and temperature dependencies of the emittance were dropped.

The ratio in brackets appearing in the first term on the right side in Eq. (7) contains the nonisothermal character of the problem with the additional assumption that the spectral emittances of the cavity walls are independent of temperature. The other four analogous equations yield the effective spectral emittance related to the variables $x1$, $z1$, $x2$, and $z2$. The angle factors $dF_{i,j}$ are defined as the fraction of the radiation emitted by an infinitesimal surface element dA_i that is directly intercepted by a surface A_j. Analytical expressions for $dF_{i,j}$ can be found in the literature.[27,28]

Because the reference temperature T_0 is not known in advance, the solution of the problem is an iterative one using adequate starting values.

Results

The pyrometer was calibrated and tested in the plasma wind tunnel with polished, fine-grained, and very pure graphite samples between 1382–1881 K. This material was chosen because it is both chemically and structurally homogeneous, and its normal spectral emittance is nearly constant (0.850) and not a function of wavelength and temperature,[15] so that the calculation of the effective emittance is not necessarily restrictive.

To avoid rapid erosion of the sample at high temperatures,[3] the tests were performed with nitrogen only. The ambient pressure was 2 mbar.

At first the pyrometer temperatures were determined from both the front and rear side of the sample (see Table 1). The front side temperature was measured with the same photoelectric pyrometer which was used to calibrate the new device. This temperature remains constant within a few Kelvin over the whole surface. The rear side temperature was measured with the minipyrometer. The signals from both pyrometers were evaluated with $\varepsilon = 0.85$.

In separated experiments under the same conditions three thermocouples were positioned in the insulation ceramics to

Table 1 Pyrometric temperatures at the front (T_f) and rear side (T_b) of the graphite sample and thermocouple temperatures inside the insulation ceramics (T_{Ki})

Nr	T_f, K	T_b, K	T_{K1}, K	T_{K2}, K	T_{K3}, K
1	1378	1384	1265	1003	673
2	1468	1467	1361	1080	761
3	1576	1574	1462	1156	842
4	1671	1654	1544	1208	886
5	1753	1725	1638	1289	949
6	1856	1821	1750	1351	1003
7	1942	1889	1822	1422	1069

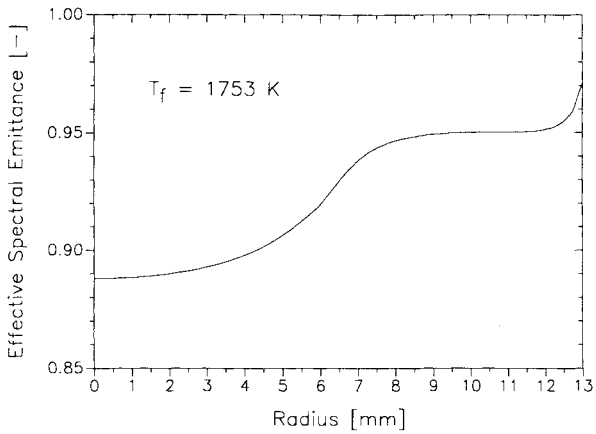

Fig. 9 Effective emittance $\varepsilon_a(r1)$.

Table 2 Data evaluation of the miniaturized pyrometer with the calculated effective emittance

Nr	$T_b(\varepsilon)$, K	$\varepsilon_a(r1 = 0)$	$T_b(\varepsilon_a)$, K	ΔT, K
1	1384	0.875	1382	2
2	1467	0.879	1464	3
3	1574	0.880	1570	4
4	1654	0.882	1649	5
5	1725	0.888	1720	5
6	1821	0.892	1814	7
7	1889	0.895	1881	8

The temperature difference is defined as $\Delta T = T_b(\varepsilon = 0.85) - T_b(\varepsilon_a)$.

obtain the temperature distribution inside the cavity (see Fig. 8): $T_{K1}(x2 = 0$ mm), $T_{K2}(x2 = 11$ mm), $T_{K3}(x2 = 22$ mm). The results show a linear decrease from $x2 = 0$ to $x2 = L_2$. The support cap (pure SiC) has a normal spectral emittance of $\varepsilon(T) = 0.80$ and the insulation ceramics $\varepsilon(T) = 0.60$. The nonisothermal effective spectral emittance ε_a was then calculated iteratively with these data.

Figure 9 shows the effective emittance of the rear side of the sample $[\varepsilon_a(r1)]$ for $T_f = 1753$ K as a function of the sample radius.

The data converged after the second iteration. The results of the true temperature are shown in Table 2. The use of an average value of 0.885 for the effective emittance at $r1 = 0$ leads to temperature values with a deviation less than ± 2 K.

As most materials investigated in the plasma wind tunnel have a normal spectral emittance in the vicinity of 0.85, the effective emittance needs to be calculated only once. Furthermore if the radiative interchanges within the enclosure would not be taken into account, the error made in the determination of the temperature would be less than 10 K.

A thermal model to calculate the temperature difference between the front and back surface of the sample in the support system is being developed.[29] Rought calculations supported by heat flux measurements show temperature differences of the same order as measured in the plasma wind tunnel with both pyrometers, when taking into account error considerations.

Conclusions

The miniaturized precision pyrometer designed for plasma wind-tunnel applications allows accurate temperature measurements at the rear side of the sample, avoiding remote measurement through the plasma flow.

The pyrometer was designed to fit standard samples for stagnation point experiments and could be easily modified for other space applications.

Radiation cavity effects were included to evaluate the true temperature accurately.

Standard electronic components were used to ensure the correct operation of the device. In a second version, which will be designed for space applications Surface-Mounted-Design components, will be included to save space and to reduce the weight load.

Acknowledgment

The authors acknowledge the supporting efforts of G. Neuer, E. Schreiber, and T. Rösgen.

References

[1]Scott, C. D., "Survey of Measurements of Flow Properties in Arc Jets," AIAA Paper 90-1765, Seattle, WA, June 1990.

[2]Auweter-Kurtz, M., Laure, S., Messerschmid, E., Röck, W., and Tubanos, N., "The IRS Plasma Wind Tunnels for the Investigation of Thermal Protection Materials for Reentry Vehicles," *Proceedings of the First European Symposium on Aerothermodynamics for Space Vehicles*, ESTEC, Noordwijk, The Netherlands, May 28–30, 1991, pp. 283–293.

[3]Auweter-Kurtz, M., Epple, J., Kurtz, H., Loesener, O., Messerschmid, E., and Mulzer, D., "Arc Heated High Enthalpy Channel for Thermal Protection Systems of Spacecraft," *Proceedings of the 4th European Symposium on Spacecraft Materials in Space Environment*, Centre d'Etudes et de Recherches de Toulouse, Toulouse, France, Sept. 6–9, 1988, pp. 75–84.

[4]Messerschmid, E., and Schöttle, U. M., "Atmospheric Reentry of Capsules and Winged Vehicles, "*Proceedings of the Space Course on Low Earth Orbit Transportation and Orbital Systems*, Forum Weltraumforschung RWTH Aachen, Aachen, Germany, March 1991, pp. 36-1–36-20.

[5]Kesselring, J. P., Maurer, R. E., Suchsland, K. E., Hartmann, G. J., and Peterson, D. L., "Arc-Heater Code-Validation Tests of Heat-Shield Materials," AIAA Paper 77-237, Jan. 1977; see also Fletcher, L. S., *Aerodynamic Heating and Thermal Protection Systems*, edited by L. S. Fletcher, Vol. 59, Progress in Astronautics and Aeronautics, AIAA, New York, 1978, pp. 261–273.

[6]Desloire, M., "Space Transportation Systems," *Proceedings of the 4th European Symposium on Spacecraft Materials in Space Environment*, Centre d'Etudes et de Recherches de Toulouse, Toulouse, France, Sept. 6–9, 1988, pp. 35–46.

[7]Bacos, M. P., and Parlier, M., "Phenomena Encountered by the Thermal Protection Materials During Hermes Reentry," *Proceedings of the 4th European Symposium on Spacecraft Materials in Space Environment*, Centre d'Etudes et de Recherches de Toulouse, Toulouse, France, Sept. 6–9, 1988, pp. 59–74.

[8]Love, T. J., "Environmental Effects on Radiation Thermometry," *Theory and Practice of Radiation Thermometry*, edited by D. P. DeWitt and G. D. Nutter, Wiley, New York, 1988, pp. 189–229.

[9]Wörner, B., "Strahlungsthermometer," *Handbuch Technik der Messung hoher Temperaturen*, Verein Deutscher Ingenieure, Düsseldorf, Germany, VDI-BW-36-19-05, March 1988, pp. BW6076-1–BW6076-25.

[10]Auweter-Kurtz, M., Habiger, H., Gogel, T., Kurtz, H., Laure, S., Loesener, O., Messerschmid, E., Röck, W., Schönemann, A., and Tubanos, N., "Plasma Wind Tunnels PWK1, PWK2," Institut für Raumfahrtsysteme, Universität Stuttgart, Stuttgart, Germany, IRS-89-P14, Jan. 1990.

[11]Chaumette, D., and Cretenet, J.-C., "Hermes Thermal Protection System Overview," International Astronautical Federation Paper 86-209, Innsbruck, Austria, Oct. 1986.

[12]Scott, C. D., and Derry, S. M., "Catalytic Recombination/Space Shuttle Heating," AIAA Paper 82-0841, St. Louis, MO, June 1982; see also *Entry Vehicle Heating and Thermal Protection Systems: Space Shuttle, Solar Starprobe, Jupiter Galileo Probe*, edited by Bauer, P. E. and Collicot, H. E., Vol. 85, Progress in Astronautics and Aeronautics, AIAA, New York, 1983, pp. 123–148.

[13]Auweter-Kurtz, M., "Qualification of Thermal Protection Systems by Laboratory Simulation Techniques," *Proceedings of the Space Course on Low Earth Orbit Transportation and Orbital Systems*, Forum Weltraumsforschung RWTH Aachen, Aachen, Germany, March 1991, pp. 39-1–39-25.

[14]Battuello, M., and Ricolfi, T., "A Technique for Deriving Emissivity Data for Infrared Pyrometry," *High Temperatures—High Pressures*, Vol. 21, No. 3, 1989, pp. 303–309.

[15]Touloukian, Y. S., and DeWitt, D. P., "Thermal Radiative Properties: Nonmetallic Solids," Vol. 8, edited by Y. S. Touloukian and C. Y. Ho, *Thermophysical Properties of Matter*, TPRC Data Series, IFI/Plenum Press, New York, 1971, pp. 8a–12a.

[16]Bedford, R. E., and Keung, M. C., "Effect of Uncertainties in Detector Responsivity on Thermodynamic Temperatures Measured with an Optical Pyrometer," *High Temperatures—High Pressures*,

Vol. 15, No. 2, 1983, pp. 119–130.

[17]Coates, P. B., "The Direct Calculation of Radiance Temperatures in Photoelectric Pyrometry," *High Temperatures—High Pressures*, Vol. 11, No. 3, 1979, pp. 289–300.

[18]Schreiber, E., "Fast Determination of Pyrometer Interference Filter Blocking," *Temperature—Its Measurement and Control in Science and Industry*, Vol. 6, American Inst. of Physics, 1992 (to be published).

[19]Schreiber, E., Neuer, G., and Wörner, B., "Performance Tests with a Standardpyrometer," *Proceedings of the 4th Symposium on Temperature and Thermal Measurement in Industry and Science*, Finnish Society of Automatic Control, Helsinki, Finland, Sept. 17–19, 1990, pp. 292–306.

[20]Nutter, G. D., "Radiation Thermometers," *Theory and Practice of Radiation Thermometry*, edited by D. P. DeWitt and G. D. Nutter, Wiley, New York, 1988, Chap. 4, pp. 231–337.

[21]Groll, M., and Neuer, G., "A New Graphite Cavity Radiator as Blackbody for High Temperatures," *Temperature—Its Measurement and Control in Science and Industry*, edited by H. P. Murray, Vol. 4, Pt. 1, Instrument Society of America, Pittsburgh, PA, 1971, pp. 449–456.

[22]Wörner, B., "A Photoelectric Direct Current Spectral Pyrometer with Linear Characteristics," *Temperature—Its Measurement and Control in Science and Industry*, edited by J. F. Schooley, Vol. 5, Pt. I, American Inst. of Physics, New York, 1982, pp. 429–432.

[23]Nutter, G. D., "Spectral-Band Radiation Thermometers," *Theory and Practice of Radiation Thermometry*, edited by D. P. DeWitt and G. D. Nutter, Wiley, New York, 1988, Chap. 5, pp. 341–458.

[24]Jung, H. C., and Verch, T., "Ein Rechenverfahren zur Auswertung pyrometrischer Messungen," *Optik*, Vol. 38, No. 1, 1973, pp. 95–109.

[25]Bedford, R. E., and Ma, C. K., "Emissivities of Diffuse Cavities: Isothermal and Nonisothermal Cones and Cylinders," *Journal of the Optical Society of America*, Vol. 64, No. 3, 1974, pp. 339–349.

[26]Sparrow, E. W., Albers, L. U., and Eckert, E. R. G., "Thermal Radiation Characteristics of Cylindrical Enclosures," *Journal of Heat Transfer*, Vol. 84, Series C, No. 1, 1962, pp. 73–81.

[27]Siegel, R., and Howell, J. R., *Thermal Radiation Heat Transfer*, 2nd ed., Hemisphere, New York, 1981, Appendixes B and C, pp. 782–831.

[28]Sparrow, E. M., and Cess, R. D., *Radiation Heat Transfer*, 2nd ed., Brooks/Cole, Belmont, CA, 1970, Chap. 4 and Appendix A, pp. 300–310.

[29]Schmidt, H. P., "Thermalhaushalt," *Handbuch der Raumfahrttechnik*, 1st ed., edited by W. Hallmann and W. Ley, Carl Hanser Verlag, Munich, 1988, Chap. 11, pp. 285–344.